CrossMark

ORIGINAL ARTICLE

Wire melting rate of alternating current gas metal arc welding

Kyungnam Kim[1] · Hyun Chung[1]

Abstract The wire melting phenomenon in alternating current gas metal arc welding (AC-GMAW) process should be carefully observed and analyzed since it is one of the most important representative characteristics of GMAW process. In this study, a new form of wire melting rate equation for AC-GMAW process is proposed based on energy conservation theory and arc physics. Using experimental data, the wire melting rate coefficients of AC-GMAW are obtained through nonlinear regression analysis. The wire melting rate is influenced not only by the current waveform, electrode polarity, and droplet size but also by the shape of the wire tip. That is, if the wire tip becomes more slender, arc heating has more influence on the wire melting. Using the wire melting rate proposed in this research, the uncertainty of calculating wire melting rate coefficients of AC-GMAW can be excluded comparing to existing method.

Keywords Wire melting rate · Alternating current gas metal arc welding · Arc behavior · Droplet

1 Introduction

Since its development process in the late 1940s [1], the process of gas metal arc welding (GMAW) has evolved considerably over the past few decades. Among the several different types of GMAW processes, alternating current gas metal arc welding (AC-GMAW) is a relatively new welding process that is gaining increased attention due to its several advantages. In AC-GMAW, direct current electrode positive (DCEP) and direct current electrode negative (DCEN) are sequentially rotated within one period of current waveform, which means it can take advantage of both positive and negative electrode polarity [2]. Since AC-GMAW exhibits characteristics of both DCEP and DCEN at the same time, it is considered as an effective and productive welding process offering advantages such as low heat input to the base metal, high wire melting rate, and stable arc.

Despite the advantages of the AC-GMAW process, it is hard to use in mild steel welding due to its insufficient penetration into the base metal. In order to overcome this problem, an improved AC-GMAW process has been developed, which has peak duration in the electrode negative (EN) period [3]. Since welding processes are usually developed through trial and error, it is hard to fully understand their characteristics before sufficient research is published. Thus, a research gap currently exists in regards to AC-GMAW process.

The wire melting rate is defined as the amount of wire mass consumed in a given unit of time during welding [4] and is one of the representative characteristics of GMAW used to assess welding process productivity. Since AC-GMAW has different wire melting rates depending on electrode polarity at a fixed current, arc length varies with polarity change and an unstable arc is produced. If the wire melting rate is known in AC-GMAW, then variation in the arc length during polarity change can be avoided by tailoring the wire feeding speed (WFS) [3]. In this way, arc stability can be attained. Wire melting rate coefficients are also needed to construct a mathematical formulation for the welding process. Arif and Chung [5] presented a force-displacement model for AC-GMAW by adopting wire melting rate coefficients of different current waveform, but they do not fit with the research due to a research gap in calculating the wire melting rate coefficients.

✉ Hyun Chung
hyunny92@kaist.edu

[1] Department of Mechanical Engineering, Korea Advanced Institute of Science and Technology (KAIST), 291, Daejeon 34141, Republic of Korea

Springer

The main objective of the present study is to develop a method for obtaining the wire melting rate coefficients of AC-GMAW, for which a new form of wire melting rate equation is proposed. With measured experimental data, the wire melting rate coefficients are obtained through nonlinear regression analysis using a new equation. The results are verified, and the arc behaviors and droplets associated with each wire melting rate are considered.

2 DCEP and DCEN

In the GMAW process, wire is melted through heat generated by electrical resistance and electrical arc heat generated between a consumable wire electrode and the workpiece [6]. In GMAW, both the wire and base metal must be connected to a power supply. Based on the type of electrode connection, the polarity falls into one of two categories: DCEP and DCEN. Welding characteristics, such as the wire melting rate and arc behavior, are changed in relation to the polarity of the connection [7].

In the case of connections in which the wire is connected to positive polarity and the base metal to negative polarity, the status of electrode connection is called DCEP or reverse polarity. Weld penetration of the base metal is deep with DCEP, because the more heat is inputted to the negative electrode. A detachment force pulls the droplet from the tip of the wire to the base metal. Therefore, the droplet is transferred to the base metal smoothly through several different metal transfer modes: short-circuit transfer, globular transfer, and spray transfer. Furthermore, since the arc is stable, a low amount of spatters is generated with DCEP [8, 9].

In the case of connections in which the wire is connected to negative polarity and the base metal to positive polarity, the status of the electrode connection is called DCEN or straight polarity. In DCEN, high wire melting rate is obtained because of climbing effect of the arc. Consequently, the same wire melting rate as DCEP can be maintained using less current in DCEN. Moreover, as there is less heat input to the base metal, weld penetration of the base metal is shallow. Since a repulsive force, which is generated by chemical reaction when CO_2 is used as shielding gas of GMAW [10], occurs that disrupts droplet detachment at the tip of the wire, the droplet does not fall onto the base metal even after sufficient growth. Because of repulsive force, the shape of droplet surface is bumpy and arc is relatively unstable [8]. For this reason, metal transfer in DCEN is mainly restricted to globular transfer mode [8, 9].

3 Improved AC-GMAW

AC-GMAW exhibits characteristics of both DCEP and DCEN at the same time. The shape of the welding current waveform

of AC-GMAW is shown in Fig. 1. The pulsed behavior of the current can be seen in both the EN period and electrode positive (EP) period. In Fig. 1, I_{p_p} means the current of positive peak, I_{p_b} means the current of positive base, I_{n_b} is the current of negative base, and I_{n_p} is the current of negative peak.

The main phenomenon of the EN period is melting of the wire. In the electrode negative base (ENB) period, a droplet formed on the tip of the wire grows slowly by a moderate arc. In the electrode negative peak (ENP) period, the increased current value causes the arc to rapidly climb up to the solid part of the wire beyond the molten droplet, as shown in Fig. 2. During this time, the surface of the wire exposed to the climbing arc is melted, but the interior of the wire is not melted. At the end of the EN period, a bulky molten droplet was formed at the tip of the wire.

In the EP period, the main phenomenon observed is detachment of the droplet, as shown in Fig. 3. In the electrode positive peak (EPP) period, the droplet formed in the EN period detached from the tip of the wire and fell to the base metal, while the arc descended along the falling droplet. At this time, the solid part of the interior of the wire is exposed. Once the droplet was detached completely, the arc reattached itself to the wire and rapidly melted the slenderized unmelted section. In electrode positive base (EPB) period, the small droplet detached and the arc was stabilized.

4 Related research

With reverse polarity, the heat generated in the cathode drop region has an insignificant influence on the melting of the electrode tip. Thus, the wire melting rate mainly depends on the heat generated by the anode voltage drop and electrical resistance of the wire.
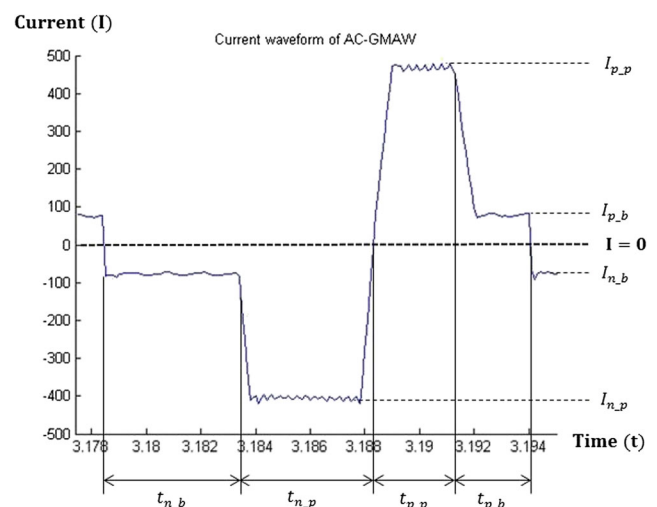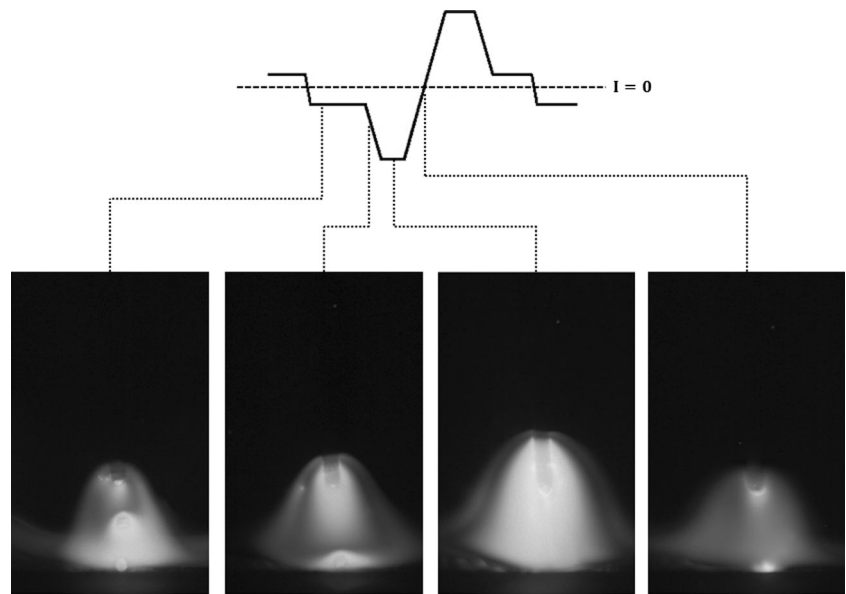

Fig. 1 Oscillogram of the current waveform of AC-GMAW

Fig. 2 Arc behavior during electrode negative period

By considering the influence of the arc and resistive heating, Lesnewich [11] developed an empirical equation for the wire melting rate in DC-GMAW:

$$MR_{dc} = \alpha I + \beta l I^2, \tag{1}$$

where MR_{dc} is the melting rate (mm/s), α is the arc melting coefficient $(mm \cdot A^{-1}s^{-1})$, β is the resistive heating coefficient $(A^{-2}s^{-1})$, I is the welding current (A), and l is the electrode extension length (mm). Note that α is dependent on the polarity, electrode material, and the anode or cathode voltage drop. The β constant depends on the electrode extension length, electrode diameter, and the resistivity of the electrode.

Calculating the wire melting rate using equation 1 is the same as obtaining the melting rate coefficients (arc melting coefficient and resistive heating coefficient). These are obtained by nonlinear regression analysis using the wire feed speed data for various current values.

Allum [12] proposed a wire melting rate for P-GMAW:

$$MR_p = \alpha I_m + \beta l\{I_m^2 + x(1-x)I_e^2\}, \tag{2}$$

where I_m is the average welding current (A), x is the peak period duration ratio, and I_e is the difference between the peak and base current $(I_p - I_b)$. From this equation, P-GMAW with a pure square pulse current waveform achieves a higher wire melting rate than DC-GMAW with the same equivalent current due to the additional term of resistive heating part. Furthermore, in P-GMAW, the wire melting rate changes with peak period duration ratio and difference between the peak and base current when at the same average current. Richardson et al. [13] enhanced the accuracy of this wire melting rate equation for P-GMAW by applying a slew rate.

As the welding current waveform becomes complicated, as is the case with AC-GMAW, welding phenomenon such as arc behavior depending on polarity also becomes more complex. In order to compute the wire melting rate coefficients of complex current waveform, a droplet burn-off rate method (DBR method) that calculates the local melting rate for each current waveform period was proposed by Harwig et al. [14]. By dividing both sides of equation 1 by the current, two components are obtained:

$$\frac{MR}{I} = \alpha + \beta lI, \tag{3}$$

where $\frac{MR}{I}$ is the burn-off rate $(mm \cdot s^{-1}A^{-1})$, and lI is the electrode extension heating factor $(mm \cdot A)$. By obtaining the burn-off rate and electrode extension heating factor for a given period of current waveform through experiment, a burn-off diagram that plots the burn-off rate against the electrode extension heating factor produces a line with a slope and y-intercept equal to the resistive heating coefficient and arc melting coefficient, respectively.

To use the DBR method, it is important to find the solid-liquid interface position through high speed video image. Solid-liquid interface represents a boundary between the solid and liquid part of the wire, and can generally be found in the area where the molten droplet starts to become larger or smaller than the diameter of the wire [1]. However, in the ENP period that is a component of the target current waveform of this research, a considerable unmelted region existed inside of the molten liquid, as shown in Fig. 4. Since the volume of this unmelted part cannot be accurately obtained, it is hard to define the solid-liquid interface position in the ENP period.

Another weakness of DBR is that when using high speed video camera, there is uncertainty as to finding the position of

Fig. 3 Arc behaviors during electrode positive period
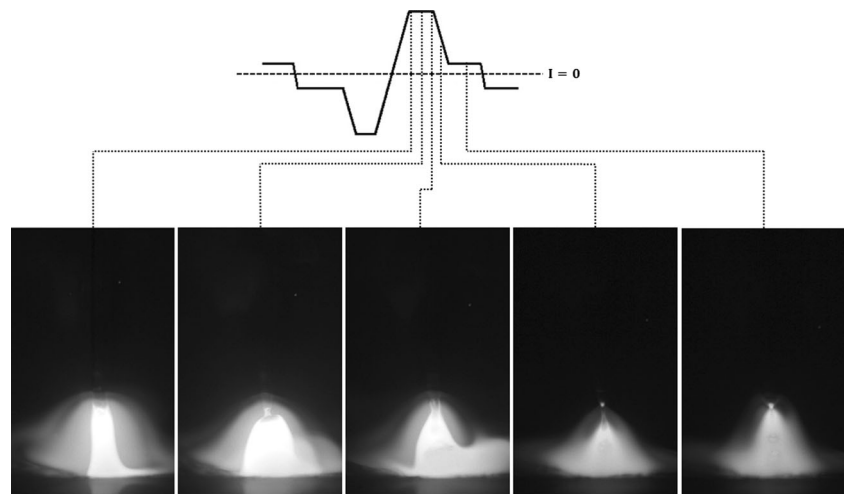
the solid-liquid interface, besides ENP period. Using DBR method, attempts were made to calculate the wire melting rate coefficients of AC-GMAW, which has peak duration in the EN period.

Figure 5 shows the results of DBR method in one experiment case with an average welding current of 150 A and an EN ratio of 44 %. In the EN period, the wire melting rate coefficients represented by the slope and y-intercept of the lines all converge; however, the result of EP period was quite variable.

Based on these results, it can be concluded that using the DBR method makes it difficult to calculate the wire melting rate of AC-GMAW due to the complicated arc behavior of the ENP period and uncertainty as to finding the position of the solid-liquid interface.

5 Experimental setup

An OTC DAIHEN DW300 power supply was used for welding. A preprogrammed current waveform algorithm built in the power supply was utilized for all experiments. During welding, the welding torch was kept immovable, and the base metal was moved by a 2-axis linear stage.

High speed videos were recorded by a Phantom Miro eX4 Mono camera at 10,000 frames per second to observe the arc behavior and electrode extension length. To record the apparent shape of the wire, a CAVILUX pulsed infrared laser backlight system was used. The exposure time was adjusted so as to record a clear image of the wire, which is in a trade-off relationship with image of arc. Typically, the exposure time was set to 2 μs, but this was changed by the surrounding environment. The laser backlight unit was synchronized to the exposure time of the camera.

The welding current and voltage data were measured by a HKS P1000 sensor, and collected using a National

Instruments PXIe-1082 chassis and DAQ board PXIe-6363 at the same frequency for each welding scenario. The WFS was measured by a HKS stationary wire sensor DV25ST-S3, and collected with a National Instruments device. The filler wire was 1.2-mm-diameter ER70S-6 mild steel, and the shielding gas flux was 20 L/min of 85Ar-15CO$_2$. Bead-on-welding was carried out using a base metal plate of SS400 steel.

To collect data for calculating the wire melting rate, AC-GMAW experiments were conducted by adjusting the value of
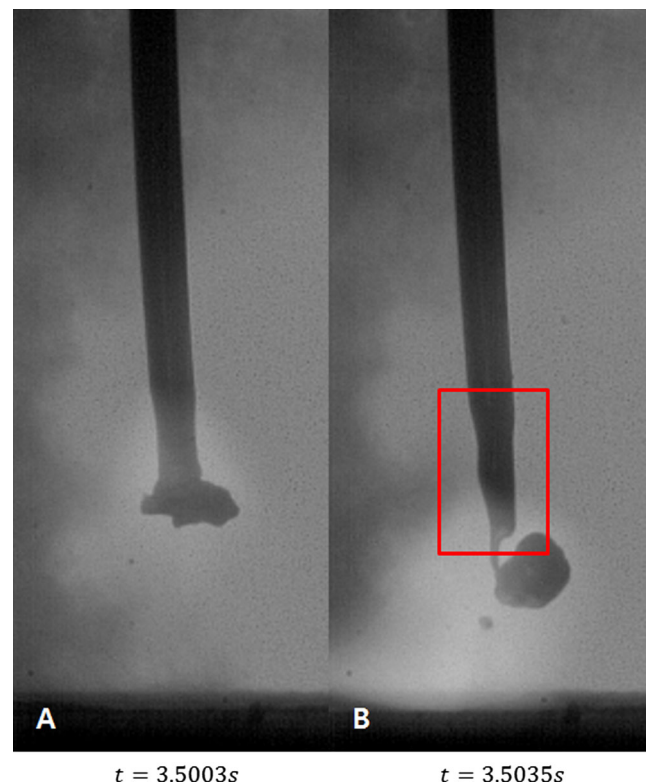

$t = 3.5003s$ $t = 3.5035s$

Fig. 4 Wire melting phenomena in electrode negative peak period and electrode positive peak period. Note: unmelted part can be observed in *red square*

(a) Results of DBR method in EN period

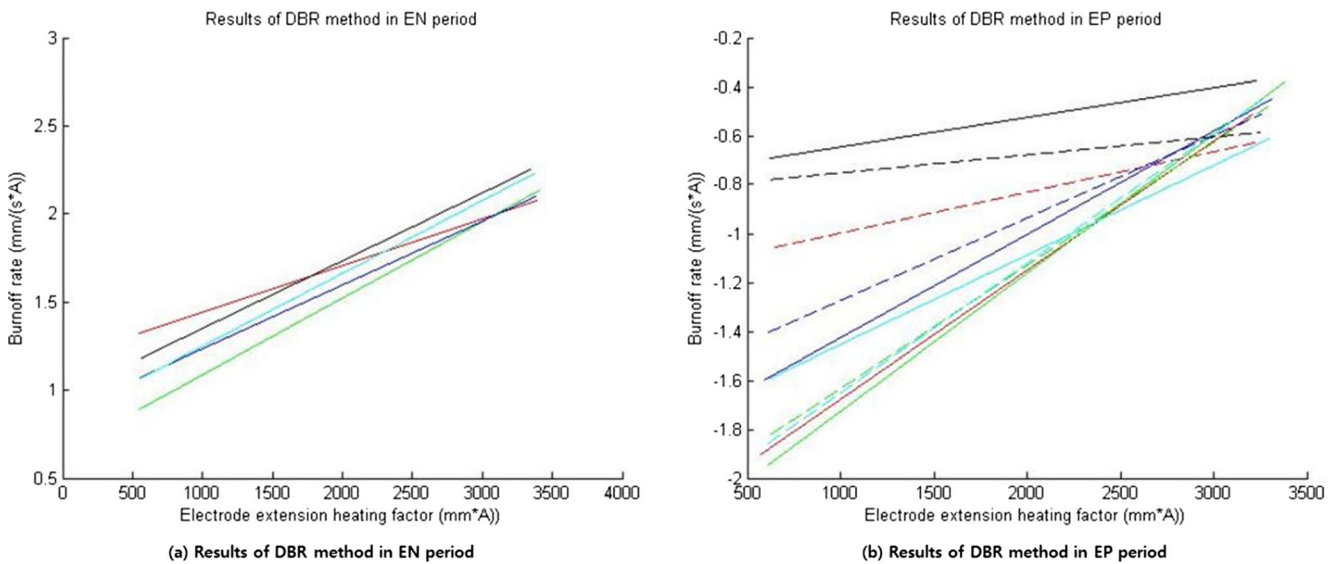(b) Results of DBR method in EP period

Fig. 5 Results of DBR method

a number of variables. Nine types of average welding current were used to cover a range of 100 to 300 A, while the EN ratio was set at 30, 37, 44, 51 or 58 %. A constant contact tip-to-work distance (CTWD) and arc voltage of 20 mm and 30 V, respectively, were used. Table 1 shows the measured average welding current and EN ratio in accordance with the set value. The first column of table shows EN ratio, and the first row of table shows average welding current. The black blocks in table are the values that cannot be set.

6 Methodology

6.1 Heat generated by the welding arc and wire melting rate in DCEN

The arc region between the electrode and base metal is broadly divided into the three regions: anode drop region, plasma region, and cathode drop region. Since the anode and cathode drop regions are both very close to their respective electrodes, the heat generated in these regions is given to the anode and cathode.

In the case of the cathode, heat is supplied from the cathode drop region. However, as electrons that are released from the cathode have thermal energy and a work function, they take away heat from cathode. It is called cooling effect. Thus, the heat absorbed by the cathode electrode is as follows [15]:

$$Q_{ca} = \left(V_{ca} - \varnothing - \frac{3}{2} \frac{kT}{e} \right) I, \tag{4}$$

where Q_{ca} is the cathode heat (J·s), and V_{ca} is the voltage drop in cathode drop region (V).

Contrary to the anode voltage drop, the cathode voltage drop is dependent on the welding current [16]. If no current flows between the anode and cathode, then the electric potential changes linearly according to position [17]. When a current flows, however, the electrons that exist between the anode and cathode affect the change in electric potential. That is, electrons around the cathode act as a shield against the electric field that is generated by anode. Consequently, as the current is increased, the electric potential around the cathode is decreased. The Child-Langmuir law describes this relationship as [17]:

$$I = \frac{4\varepsilon_0}{9} \sqrt{\frac{e}{m}} \frac{V^{3/2}}{d^2}, \tag{5}$$

where ε_0 is the dielectric constant in a vacuum (F/m), m is the mass of an electron (kg), and d is the thickness of the cathode drop region (m). With regards to d, since the thickness of the cathode drop region is generally less than 0.1 mm, it can be reasonably regarded as being one-dimensional [18]. The relationship between the welding current and cathode drop voltage is therefore given as:

$$V_{ca} \propto I^{2/3}. \tag{6}$$

Considering the relationship between the welding current and cathode drop voltage, then the cathode heat can be expressed by the following equation:

$$Q_{ca} = \text{Constant}_1 \times I^{5/3} + \text{Constant}_2 \times I. \tag{7}$$

In DCEN, the electrode is melted by the heat that is generated by the resistance of the electrode and the cathode voltage

Table 1 Set values of experiment for nonlinear regression analysis

Setting	100 A	125 A	150 A	175 A	200 A	225 A	250 A	275 A	300 A
30 %		129 A-32 %	146 A-29 %	171 A-30 %	195 A-30 %	215 A-30 %			
37 %	107 A-37 %	129 A-37 %	149 A-38 %	172 A-37 %	200 A-37 %	212 A-37 %	229 A-38 %	252 A-38 %	
44 %	104 A-44 %	128 A-44 %	149 A-44 %	173 A-44 %	201 A-45 %	215 A-44 %	234 A-44 %	261 A-45 %	273 A-44 %
51 %	104 A-51 %	127 A-51 %	148 A-51 %	171 A-51 %	193 A-51 %	214 A-51 %	240 A-51 %	258 A-51 %	277 A-51 %
58 %	108 A-58 %	132 A-58 %	150 A-58 %	172 A-58 %	193 A-58 %	215 A-58 %	240 A-57 %	262 A-57 %	279 A-57 %

drop. The total heat absorbed by the electrode can therefore be expressed as:

$$Q_{total} = Q_{ca} + Q_{joule}$$
$$= \left(V_{ca} - \varnothing - \frac{3}{2}\frac{kT}{e}\right)I + \left(\frac{1}{\pi R_e^2 \sigma}\right)lI^2$$
$$= \left(Constant_1 \times I^{5/3} + Constant_2 \times I\right)$$
$$+ \left(Constant \times l \times I^2\right). \tag{8}$$

From the above equation, the wire melting rate equation can be derived as:

$$MR_{en} = \alpha_n I^{5/3} + \gamma_n I + \beta_n lI^2, \tag{9}$$

where MR_{en} is the melting rate of DCEN (mm/s), and α_p and γ_n are the arc melting coefficients of DCEN with units of $mm \cdot A^{-5/3} s^{-1}$ and $mm \cdot A^{-1} s^{-1}$, respectively. The variable β_p is the resistive heating coefficient of DCEN ($A^{-2} s^{-1}$).

6.2 Wire melting rate equation for AC-GMAW

By considering the welding current as a time-dependent variable, the wire melting rate equations for the EN and EP periods can be derived by integrating and averaging over one pulse cycle of the wire melting rate equation of DC-GMAW.

$$MR_{AC\_p} = E\left(\int \alpha_p I(t) + \beta_p l_p I(t)^2 dt\right)$$
$$= \alpha_p \bar{I}_{p-} + \beta_p l_p \left\{\bar{I}_p^2 + x_p(1-x_p)I_{p\_e}^2\right\} \tag{10}$$

$$MR_{AC\_n}$$
$$= E\left(\int \alpha_n I_n^{5/3}(t) + \gamma_n I(t) + \beta_n l_n I(t)^2 dt\right)$$
$$= \alpha_n \bar{I}_n^{5/3} + \gamma_n \bar{I}_{n-} + \beta_n l_n \left\{\bar{I}_n^2 + x_n(1-x_n)I_{n\_e}^2\right\} \tag{11}$$

By combining the wire melting rate equations for the EN and EP periods, a new form of wire melting rate equation for calculating the wire melting rate coefficients of AC-GMAW is derived. Since the wire melting rate is defined as the amount of wire mass consumed in a given unit of time during welding, components representing the wire melting rate of the EN and EP periods are weighted by the EN period duration ratio (t_n) and EP period duration ratio ($1-t_n$), respectively:

$$WMR_{AC}$$
$$= t_n\left[\alpha_n \bar{I}_n^{5/3} + \gamma_n \bar{I}_{n-} + \beta_n l_n\left\{\bar{I}_n^2 + x_n(1-x_n)I_{n\_e}^2\right\}\right]$$
$$+ (1-t_n)\left[\alpha_p \bar{I}_{p-} + \beta_p l_p\left\{\bar{I}_p^2 + x_p\left(1-x_p\right)I_{p\_e}^2\right\}\right], \tag{12}$$

where t_n is the electrode negative period duration ratio, α_n and γ_n are the arc melting coefficients of the EN period, α_p is the arc melting coefficient of the EP period, and β_n and β_p are the resistive heating coefficients of the EN and EP period, respectively. I_n and I_p are the average currents of the EN and EP period, respectively. $I_n^{5/3}$ is the average value of 5/3 square of the current in EN period. It is related to the dependent relationship between welding current and cathode drop voltage. I_{n_e} and I_{p_e} are the differences between the base and peak current of the EN and EP period, l_n and l_p are the electrode extension lengths of the EN and EP period, and x_n and x_p are the fractional peak durations of the EN and EP period. Note that the equation consists of two sections: one representing the wire melting rate of the EN period (indicated by the subscript "n"), and the other the wire melting rate of the EP period (subscript "p").

In this equation, the values of the eleven variables (WMR_{AC}, t_n, $I_n^{5/3}$, I_n, $\bar{I}_p$, I_{n_e}, I_{p_e}, x_n, x_p, l_n, and l_p) are measured during experiments, and the five parameters (α_n, γ_n, β_n, α_p, and β_p) are determined by nonlinear regression analysis.

The EN period duration ratio is calculated by following equation:

$$t_n = \frac{t_{n\_b} + t_{n\_p}}{(t_{n\_b} + t_{n\_p}) + (t_{p\_p} + t_{p\_b})}. \tag{13}$$

The peak current and base current ($I_{n\_b}, I_{n\_p}, I_{p\_p}$, and I_{p_b}) are defined as the average current value of the period in which the current is constant, as shown in Fig. 1.

The fractional peak duration (x_n, x_p) is the ratio occupied by the peak for each period:

$$x_{(n,\ p)} = \frac{t_{(n,\ p)\_p}}{t_{(n,\ p)\_p} + t_{(n,\ p)\_b}}. \tag{14}$$

When nonlinear regression analysis is conducted, the average values for the measured wire feeding speed with each case of AC-GMAW are used for WMR$_{AC}$.

7 Results and discussion

In AC-GMAW, there is the ENP period in which the arc rapidly climbs up to the solid part of the wire beyond the molten droplet and supplies heat to the electrode surface. As the surface of the wire exposed to the climbed arc is melted, but the interior of the wire is not. Like this, slenderized section of wire is formed. Since increasing the current in the ENP period causes the arc to climb higher, the slenderized section is extended.

The slenderized section affected the wire melting rate. Therefore, in order to observe the effect of ENP period current on wire melting rate, the experiments were divided into three groups based on the ENP period current, and the wire melting rate coefficients for each group were calculated. As shown in Fig. 6(b), experiments in which the ENP period current was less than 340 A made up the first group. The second group
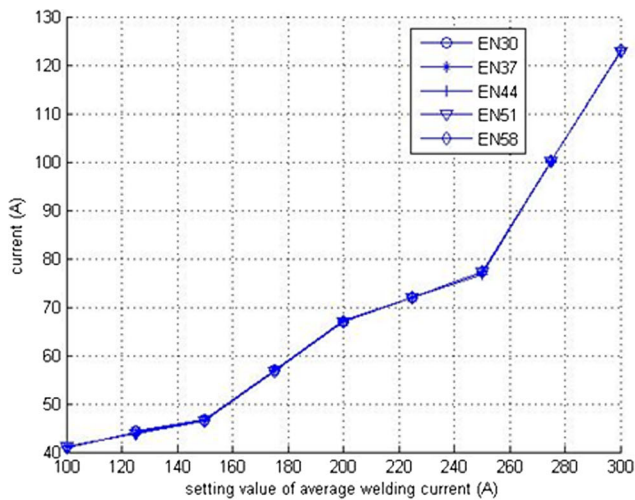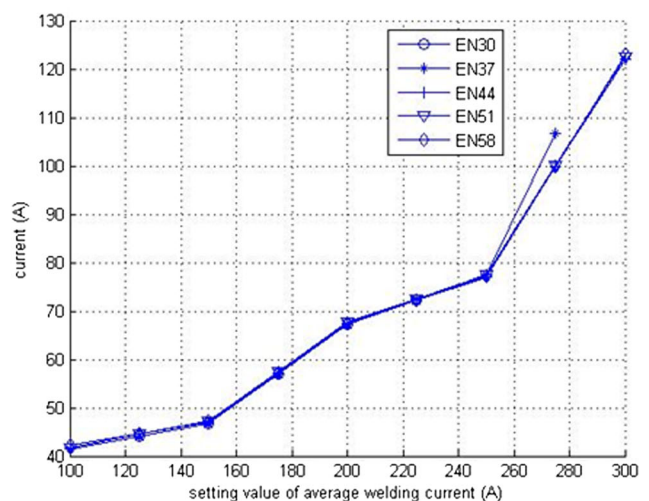

(a) Negative base current
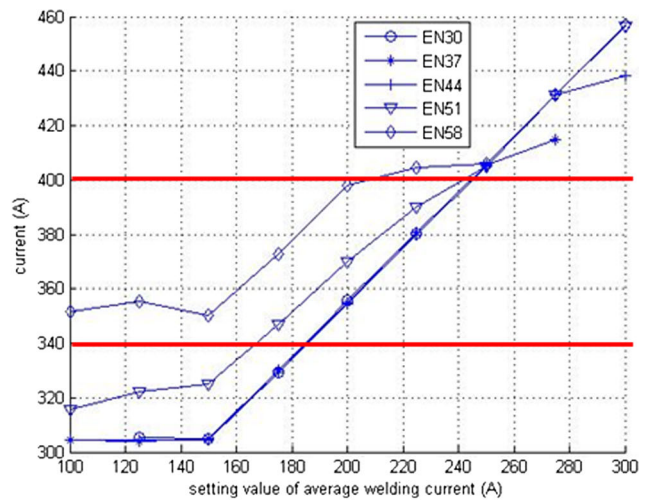
(b) Negative peak current
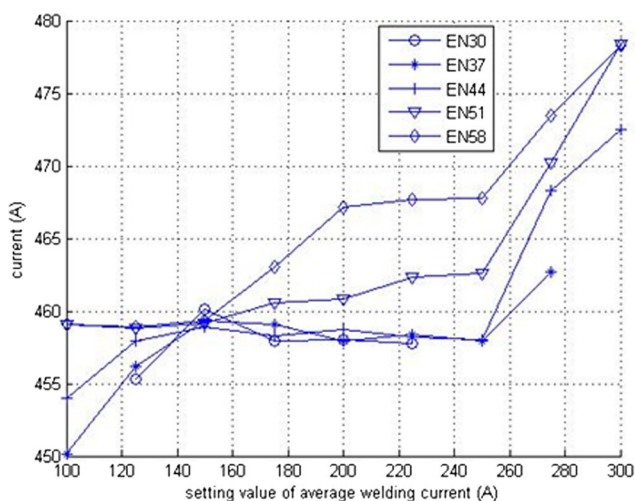
(c) Positive peak current

(d) Positive base current
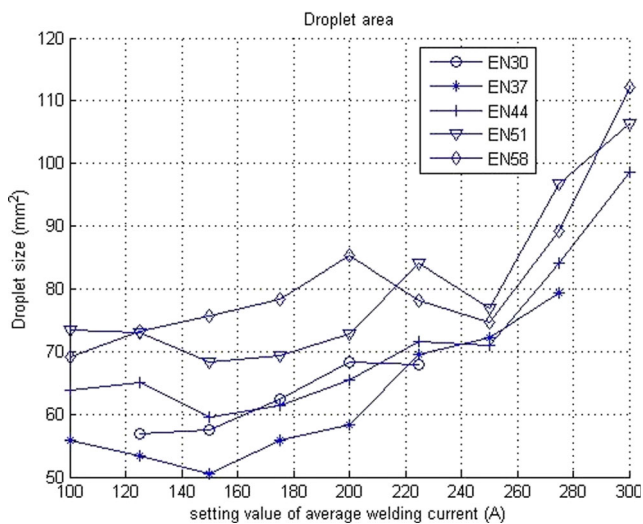
Fig. 6 Current for each period

Fig. 7 Droplet area at the end of the ENB period

criterion was a current of more than 340 A but less than 400 A, while the third group had a current of more than 400 A.

The wire melting rate coefficients (arc melting coefficients and resistive heating coefficient) were calculated using the newly proposed wire melting rate equation. When the ENP period current was less than 340 A, α_n is 0.0283 $\mathrm{mm \cdot A^{-5/3} s^{-1}}$, γ_n is −6.50E-13 $\mathrm{mm \cdot A^{-1} s^{-1}}$, β_n is −0.0002265 $\mathrm{A^{-2} s^{-1}}$, α_p is 0.2659 $\mathrm{mm \cdot A^{-1} s^{-1}}$, and β_p is 0.0000974 $\mathrm{A^{-2} s^{-1}}$. When the ENP period current was more than 340 A but less than 400 A, α_n is 0.0137 $\mathrm{mm \cdot A^{-5/3} s^{-1}}$, γ_n is −4.39E-11 $\mathrm{mm \cdot A^{-1} s^{-1}}$, β_n is 0.0000500 $\mathrm{A^{-2} s^{-1}}$, α_p is 0.6439 $\mathrm{mm \cdot A^{-1} s^{-1}}$, and β_p is −0.0000136 $\mathrm{A^{-2} s^{-1}}$. When the ENP period current was more than 400 A, α_n is 0.0057 $\mathrm{mm \cdot A^{-5/3} s^{-1}}$, γ_n is −3.67E-07 $\mathrm{mm \cdot A^{-1} s^{-1}}$, β_n is 0.0001230 $\mathrm{A^{-2} s^{-1}}$, α_p is 0.7498 $\mathrm{mm \cdot A^{-1} s^{-1}}$, and β_p is −0.0000196 $\mathrm{A^{-2} s^{-1}}$.
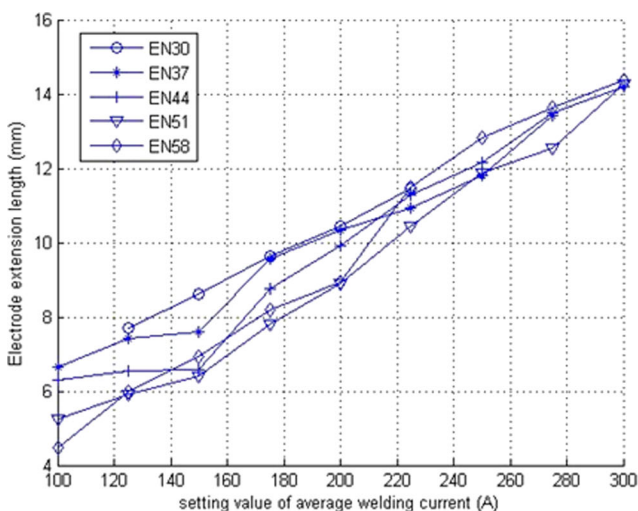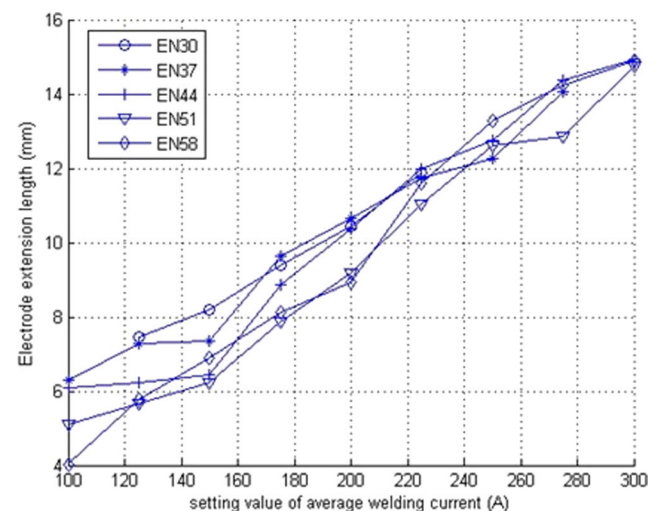
In the EN period, the arc melting coefficients (α_n and γ_n) both decreased due to the droplet size and related characteristic of the arc. After droplet detachment, virgin wire is directly exposed to the arc and is quickly melted, resulting in faster droplet growth. However, this droplet inhibits arc concentration on the wire, as the arc root is located on the bottom of droplet. Consequently, the melting rate caused by arc is decreased [14]. In Fig. 7, the droplet area recorded by high speed video increased as the average welding current was increased, and so as the average welding current was increased, α_n and γ_n decreased.

The resistive heating coefficient (β_n) increased in the EN period. β_n implies wire melting occurred by resistive heating in EN period. This, in turn, is affected by the wire diameter and electrode extension length.

In Fig. 8(a), it can be seen that as the average welding current increases, the electrode extension length also increases. This increases the resistive heating generated in wire increased, and for this reason, β_n increased.

In the EP period, the change in the arc melting coefficient (α_p) and resistive heating coefficient (β_p) was the complete opposite of that for EN period. α_p increased as the average welding current increased. In the ENP period, the arc rapidly climbed up to the solid part of the wire beyond molten droplet, and though the wire surface exposed to the climbed arc was melted, the interior of the wire was not. In this way, a slenderized section of wire was formed. In the EPP period, the detachment of the droplet allows the arc to supply heat to the wire, resulting in the rapid melting of slenderized section. Thus, if a slenderized section exists, the magnitude of the arc melting coefficient is increased [13].

Figure 9 shows a tendency of measured length and diameter of the slender section. And the exterior of slenderized wire at 58 % EN ratio are shown in Fig. 10. Note that as the average

(a) Electrode extension length at EN period

(b) Electrode extension length at EP period

Fig. 8 Electrode extension lengths in EN period and EP period

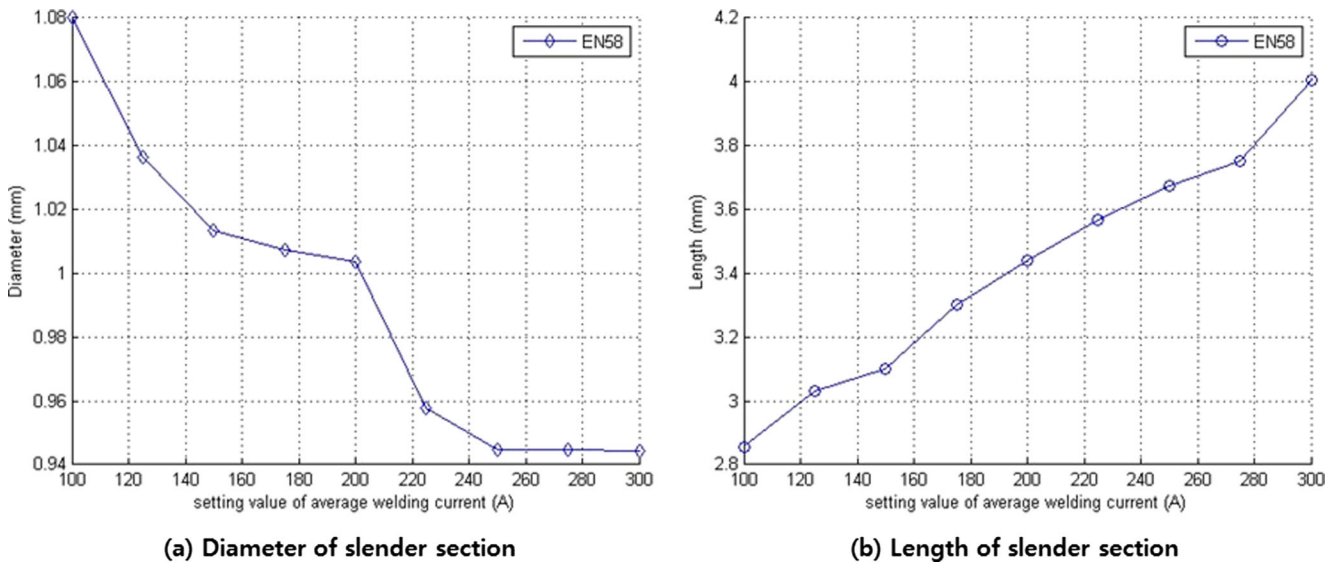(a) Diameter of slender section

(b) Length of slender section

Fig. 9 Diameter and length of slender section

welding current is increased, the slenderized section increases in length but decreases in diameter, which increases the melting effect of the arc. As a result, α_p is increased in the EP period when the average welding current is increased.

In the EP period, the electrode extension length increased when the average welding current was increased, but β_p was decreased. This was an opposite result to the EN period. Because the slenderized section is just a small part of the electrode, it does not affect the total resistive heating of the wire. However, amount of melting by arc is increased due to the slenderized section being extended. Since this phenomenon does not being contained in wire feeding speed used for nonlinear regression analysis, the effect of resistive heating seems to be decreased due to the increased effect of arc heating. For this reason, despite the increasing electrode extension length, β_p decreased.

Figure 11 shows the relationship between the measured wire feeding speed and the calculated wire melting rate. The coefficient of correlation R was 0.99, and the standard error was 0.47. This means that the new wire melting rate equation suitably calculates the arc melting coefficients and resistive heating coefficients.

The obtained wire melting rate coefficients were verified using seven sets of experimental data, which were not used in the nonlinear regression analysis.

Figure 12 and Table 2 show the results of verification. The calculated wire melting rates were very close to the measured wire feeding speed. The highest error rate was 5.27 % when the average current was set to 100 A and the EN ratio was 49 %. This means that using the arc melting coefficients and resistive heating coefficient obtained by the proposed wire melting rate equation allows the wire melting rate of AC-GMAW to be predicted.

8 Conclusions

The AC-GMAW, which has a pulsed behavior of current waveform in both the EN and EP periods, has noticeable characteristics. In the ENP period, the arc rapidly climbs up to the solid part of the wire beyond the droplet. Since the surface of the wire exposed to this climbed arc is melted, additional wire melting occurs. But the interior of the wire is not melted. As a result, a large amount of unmelted solid part and melted liquid
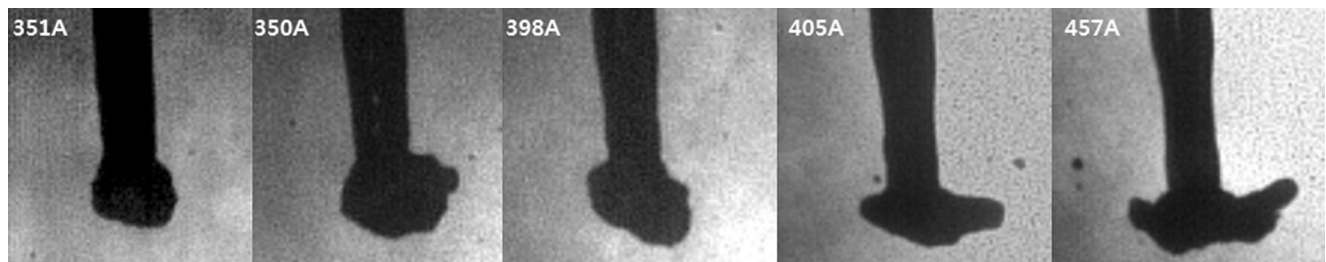

Fig. 10 Slender sections of various average welding currents at 58 % EN ratio
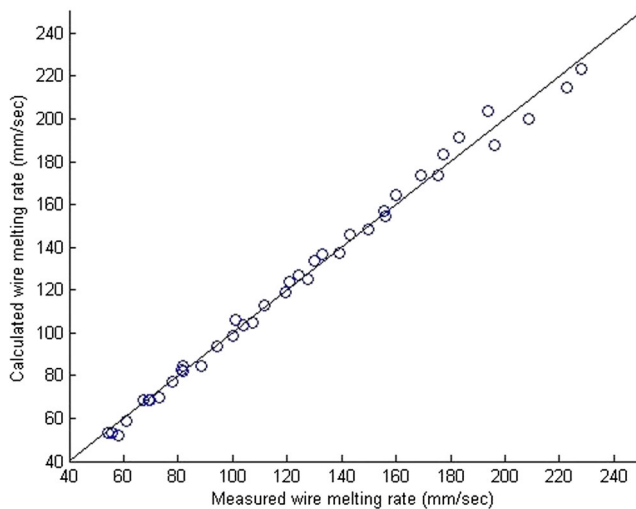
Fig. 11 Relationship between measured wire feeding speed and calculated wire melting rate
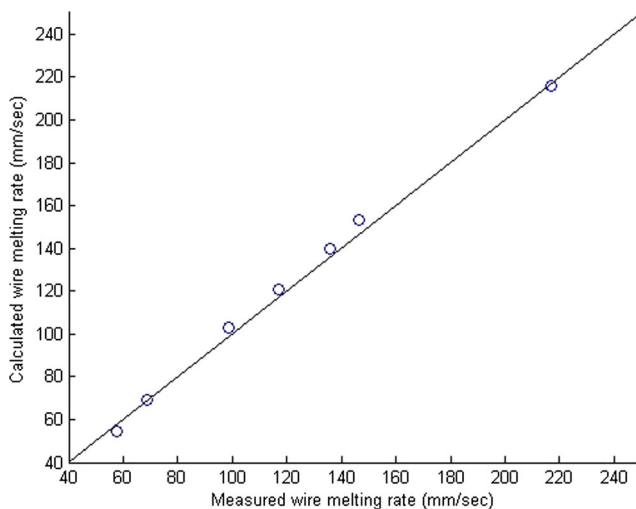

Fig. 12 Plot of measured wire feeding speed and calculated wire melting rate of experiments for verifying

This research proposes a new wire melting rate equation that reflects the physical properties of DCEN. A new wire melting rate equation for AC-GMAW was also derived by merging the wire melting rate equations of DCEN and DCEP. Owing to the complex arc behavior during the ENP period, the respective accurate wire melting rates for the EN and EP period could not be obtained. Therefore, the wire melting rate coefficients were calculated by using the average wire feeding speed of several cycle of welding current waveform and the new wire melting rate equation for AC-GMAW through nonlinear regression analysis.

The proposed wire melting rate equation of AC-GMAW was verified by using obtained wire melting rate coefficients and experimental data, which was not used for nonlinear regression analysis. In conclusion, the calculated wire melting rate and measured wire feeding speed were reasonably matched.

Using the wire melting rate equation proposed in this research, the uncertainty of calculating wire melting rate coefficients of AC-GMAW can be excluded comparing to existing method. Also, even if the wire melting rate of certain period, which has complex arc behavior, cannot be obtained, the wire melting rate coefficients of AC-GMAW can be calculated using average wire feeding speed.

The wire melting rate coefficients of AC-GMAW can be calculated by using wire melting rate equation proposed in this research. Therefore, it is possible to perform welding at the intended wire melting rate by setting the variable to suit the working environment. Moreover, since the research gap of wire melting rate is filled, related research of AC-GMAW can be extended. Furthermore, AC-GMAW process could be implemented in industry.

In the ENP period of AC-GMAW, the unmelted part exists in the interior of wire. The volume of unmelted part cannot be accurately obtained by using high speed video. After the ENP period, the arc is descended following detached droplet in EPP period. At the EPP period, the molten part of near the solid-liquid interface is partially solidified. This phenomenon is not contained in the wire melting rate equation. Therefore, if the volume of unmelted part in the interior of wire can be measured and additional term, which contains solidification phenomenon, is added to the wire melting rate equation, the local wire melting rate coefficients of each period of the current waveform of AC-GMAW can be calculated. This is an

part coexist in the same region. The wire melting rate is influenced by the current waveform, electrode polarity, droplet size, and the shape of the wire tip. That is, if the wire tip becomes more slender, arc heating has more influence on the wire melting.

Table 2 Measured wire feeding speed and calculated wire melting rate of experiments for verifying		100 A 49 %	125 A 40 %	175 A 27 %	200 A 25 %	225 A 35 %	250 A 34 %	300 A 46 %
	Measured WFS (m/min)	57.5563	68.7408	98.6191	116.945	135.759	146.683	216.760
	Calculated WMR (m/min)	54.5256	69.1521	102.854	121.009	139.815	153.139	215.853
	Error rate (%)	5.27	0.60	4.29	3.47	2.99	4.40	0.42

unexplored area for future research of the wire melting rate equation of AC-GMAW.

References

1. Soderstrom EJ (2007) Gas metal arc-welding electrode heat-and-mass transfer mechanisms. Ph.D. Dissertation, Department of Metallurgical and Mechanical Engineering, Colorado School of Mines, Golden, Colorado, USA
2. Ueyama T, Tong H, Yazawa I, Hirami M, Kihara T, Nakata K, Ushio M (2004) Aluminum alloy sheet welding by the laser AC pulsed MIG hybrid process. Weld Int 18(5):345–350
3. Arif N, Chung H (2015) Alternating current-gas metal arc welding for application to thick plates. J Mater Process Technol 222:75–83
4. Singh D, Bhardwaj P, Yang YD, McLean A, Hasegawa M, Iwase M (2010) The influence of carbonaceous material on the melting behaviour of mould powder. Steel Research International 81(11):974–979
5. Arif N, Chung H (2014) Alternating current-gas metal arc welding for application to thin sheets. J Mater Process Technol 214(9):1828–1837
6. Andrade RC, Carvalho GCD (2013) Development of software for slicing 3D shell-like computational model and for off-line generation robot trajectory for building metallic parts by means of 564 layered gas metal arc welding. 22nd International Congress of 565 Mechanical Engineering (COBEM 2013), November 3-7, Ribeirão Preto, SP, Brazil
7. Park HJ, Kim DC, Kang MJ, Rhee S (2013) The arc phenomenon by the characteristic of EN ratio in AC pulse GMAW. Int J Adv Manuf Technol 66:867–875
8. Talkington JE (1998) Variable polarity gas metal arc welding. Masters Dissertation, Department of Material Science and Engineering, Ohio State University, Columbus, Ohio, USA
9. Vilarinho LO, Nascimento AS, Fernandes DB, Mota CAM (2009) Methodology for parameter calculation of VP-GMAW. Weld J 88(4):92–98
10. Lancaster JF (1986) The physics of welding, 2nd edn. Pergamon Press, New York, p. 214
11. Lesnewich A (1958) Control of melting rate and metal transfer in gas-shielded metal arc welding— part 1—control of electrode melting rate. Weld J 37(8):343–353
12. Allum CJ (1983) MIG. welding—time for a reassessment. Metal Construction 15:347–353
13. Richardson IM, Bucknall PW, Stares I (1994) The influence of power source dynamics on wire melting rate in pulsed GMA welding. Weld J 73:32–37
14. Harwig DD, Dierksheide JE, Yapp D, Blackman S (2006) Arc behavior and melting rate in the VP-GMAW process. Weld J 85(3):52–62
15. Lancaster JF (1986) The physics of welding, 2nd edn. Pergamon Press, New York, p. 250
16. Lesnewich A (1987) Commentary: mathematical modeling of melting rates for submerged-arc welding. Weld J 66(12):386–387
17. Greene D (2001) The Langmuir-Child law and the work function of tungsten. Laboratory report, Department of Physics and Engineering Physics, University of Saskatchewan. http://physics.usask.ca/~angie/p404/reports/exp3/p404-langmuirchild-lab3.doc. Accessed 17 September 2016
18. Zhu P, Lowke JJ, Morrow RHNR (1992) A unified theory of free burning arcs, cathode sheaths and cathodes. J Phys D Appl Phys 25(8):1221–1230